

Article

Physicochemical Characterization, Thermal Behavior, and Pyrolysis Kinetics of Sewage Sludge

Hanane Messaoudi ^{1,2}, Abdelghani Koukouch ², Ilias Bakhattar ¹, Mohamed Asbik ¹, Sylvie Bonnamy ³, El Ghali Bennouna ², Toufik Boushaki ^{4,*}, Brahim Sarh ⁴ and Abel Rouboa ⁵

¹ Thermal and Energy Research Team, Ecole Nationale Supérieure d'Arts et Métiers, Mohammed V University in Rabat, Rabat 10000, Morocco; hanane_messaoudi@um5.ac.ma (H.M.)

² Green Energy Park (IRESEN, UM6P), Ben Guerir 43150, Morocco

³ Laboratory of Confinement, Materials and Nanostructures (ICMN)-CNRS UMR7374, 45071 Orleans Cedex 2, France

⁴ Institute of Combustion, Aerothermal, Reactivity and Environment (ICARE)-CNRS UPR3021, 45071 Orléans Cedex 2, France

⁵ Faculty of Engineering, University of Porto, Rua Dr. Roberto Frias, 4200-465 Porto, Portugal

* Correspondence: toufik.boushaki@cnrs-orleans.fr

Abstract: Pyrolysis is an energy recovery technique with significant potential for managing wastewater treatment plant byproducts. This research aims to investigate the physicochemical and thermal properties of Moroccan sludge, as well as the behavior of its decomposition during pyrolysis at three different heating speeds (5, 10, and 20 K/min). Characterization of the sludge before pyrolysis through ultimate analysis, proximate analysis, FTIR spectroscopy, and XRD revealed that the sludge consists predominantly of organic matter, with a volatile matter rate of 48%, an ash rate of 37%, and a higher heating value (HHV) of 15 MJ/kg. The TGA-DTG curves identified four distinct stages in the sludge decomposition process: drying, decomposition of organic matter, degradation of calcium carbonate, and decomposition of inorganic matter. Using TG-MS analysis, the principal gases identified during pyrolysis were H₂O, H₂, CH₄, CO₂, CO, NO, and SO. The average activation energies (E_a) determined through kinetics models were found to be 413.4 kJ/mol for the Kissinger–Akahira–Sunose (KAS) model, 419.6 kJ/mol for the Flynn–Wall–Ozawa (FWO) model, and 416.3 kJ/mol for the Starink model. The values of E_a and the pre-exponential coefficient (A) obtained through the KAS, FWO, and Starink techniques are consistent with ΔG values ranging between 152 and 155 KJ/mol. The positive ΔS values range from 0.003 to 1.415 kJ/mol.K, indicating the complexity of the sludge response during pyrolysis and the spontaneity of the chemical reaction at high temperatures. The kinetic data obtained serves as a pillar for the development and improvement of sewage sludge pyrolysis systems, reinforcing their role in sustainable energy production.

Keywords: sewage sludge; physicochemical analyses; thermal analysis; pyrolysis kinetic



Citation: Messaoudi, H.; Koukouch, A.; Bakhattar, I.; Asbik, M.; Bonnamy, S.; Bennouna, E.G.; Boushaki, T.; Sarh, B.; Rouboa, A. Physicochemical Characterization, Thermal Behavior, and Pyrolysis Kinetics of Sewage Sludge. *Energies* **2024**, *17*, 582. <https://doi.org/10.3390/en17030582>

Academic Editor: Fernando Rubiera González

Received: 8 December 2023

Revised: 20 January 2024

Accepted: 23 January 2024

Published: 25 January 2024



Copyright: © 2024 by the authors. Licensee MDPI, Basel, Switzerland. This article is an open access article distributed under the terms and conditions of the Creative Commons Attribution (CC BY) license (<https://creativecommons.org/licenses/by/4.0/>).

1. Introduction

Morocco, in recent years, has experienced a significant increase in the number of wastewater treatment plants (21 WWTP in 2005 to 153 WWTP in 2020) according to Ministry of Energy Transition and Sustainable Development, 2021. These plants produce a huge quantity of sewage sludge, about 110,000 million tons of dry matter in 2020 [1], that must be managed. Wastewater treatment causes a concentration of several hazardous chemical and biological elements in the sludge, like microorganisms, and harmful components such as heavy metals, organic compounds, dioxins, chemicals, and pharmaceuticals. Those elements pose challenges and difficulties in terms of the disposal and management of such waste [2,3].

Currently, sludge disposal is most often done by landfilling, which causes a risk to the environment because of the pollution of the water table by the leachate of sludge and the

production of uncontrolled methane by the greenhouse effect [4]. The reuse of sludge in agriculture is one of the disposal routes adopted at an international level, but in Europe, for example, this route is becoming increasingly limited and prohibited according to the European Directive 86/278/EEC because of the contamination of soil and groundwater by heavy metals, the thing that will subsequently affect human and animal health.

The latest researches are focused on the energy recovery of sewage sludge, as a type of biomass to convert it into products with high energetic value such as biochar, bio-oil, and synthesis gas, especially as the energy demand is still growing, mainly at the industrial level [5,6]. The energetic valorization of a biomasses can be generally performed with biochemical methods or with thermochemical processes. Biochemical conversions of sewage sludge, such as anaerobic digestion, take time and require high cost enzymes for the decomposition of organic matter [7,8]. In contrast, thermochemical methods such as pyrolysis, gasification, and combustion, can strongly reduce the volume of sludge, can thermally destroy the toxic organic matter present in sludge, as well as lead to energy recovery with different forms [9–11].

Among the thermochemical processes that have caught the attention of researchers and scientists is pyrolysis [12]. It is a thermal degradation of a material in the absence of oxygen that offers an alternative way for stable treatment of solid waste. This method is still in the research and development phase because of its complexity [12], especially with such a complex compound as sewage sludge. Some studies have been carried out on the physicochemical and thermodynamic characterization of sludge, its behavior during pyrolysis, and its thermal kinetics.

Shahbeig and Nosrati (2020) [13], carried out an extensive study on the pyrolysis of Iranian sewage sludge using TG-DTG analysis to determine its bioenergy potential. They describe the pyrolytic behavior of the sludge as following three stages: at first moisture release occurs, followed by the degradation of organic substances, then by the decomposition of the char in a third stage. They also performed a thermokinetic study with three bioconversion models: FWO, KAS and Starink. The calculated values of activation energy (126.62–136.92 kJ/mol), Gibbs energy (159.19–159.61 kJ/mol), and higher heating values (16.47 ± 0.03 MJ/kg) showed that the sludge has a bioenergetic potential. Also, the positive values of ΔG and the negative values of ΔS showed that the chemical reaction of the sludge during the pyrolysis is not spontaneous.

More recently, Mphahlele et al. (2021) [14] conducted a study on the slow pyrolysis with a heating rate of 10, 20, and 30 K/min of sewage sludge from South Africa (Gauteng). They focused on the characteristics of this waste during its decomposition using infrared spectroscopy (FTIR) analysis. The results showed the disappearance of volatile organic compounds and the formation of aromatic structures. The TG-DTG analysis indicated three stages during pyrolysis: dehydration, devolatilization, and slow pyrolysis stage. They studied the thermal kinetics with FWO, KAS, and Starink models. The determination of thermodynamic parameters showed that the reaction chemistry during pyrolysis is complex and that the organic compounds contained in the sludge volatilized rapidly with high and low temperatures. The Z-master plots method of Criado (1978) [15] was performed in this study to locate the dominance of reaction patterns with the conversion rate.

Fonts et al. (2009) [16] studied the pyrolysis of Spanish sludge in a fluidized bed reactor and showed that non-standardized wastewater treatment methods in wastewater treatment plants (WWTP) can change the chemical composition of the sludge, which affects the products formed after pyrolysis and their characteristics. They also found that the ash content of the sludge has a great influence on the pyrolysis: the higher the ash content, the higher the gas yield, and the lower the yield of liquids and solids.

Naqvi et al. (2018) [17] examined the thermokinetic and thermodynamic properties of high ash sewage sludge during pyrolysis by thermogravimetric analysis, and used the Coats–Redfern method for the determination of activation energy and pre-exponential factor. They outlined that the pyrolysis of sewage sludge can be divided into three decomposition stages and that the low-temperature stable components degrade in the temperature

range of 250–450 °C while the high-temperature stable components decompose in the range of 450–700 °C.

Zhai et al. (2012) [18] and Shao et al. (2008) [19] conducted a study to characterize and determine the kinetic properties of sewage sludge during pyrolysis at different heating rates. The results showed that the mass loss of sludge is distinct in three stages and the pyrolysis characteristics of sludge differ because of their nature and their origin in the wastewater treatment processes [19]. FTIR analysis revealed the presence of functional groups such as NH, C-H, and C=C in the sludge, which indicates compositional similarity with natural materials such as lignocellulose, cellulose, and lignin [18], and indicated that the pyrolysis gas of the sludge was mainly composed of CO, CO₂, CH₄, light hydrocarbons, and also hydrogen, which was detected using Outokumpu HSC Chemistry version 4.1 software [19].

The goal of the present work on the pyrolysis of Moroccan sewage sludge was to investigate more accurately the thermal decomposition of these wastes, their physico-chemical characteristics before, during, and after the pyrolysis, as well as thorough an understanding of their thermal kinetics and their thermodynamic parameters. It is necessary to develop a rich literature on pyrolysis which is a complicated process, especially with such a complicated biomass as sewage sludge that has a chemical composition that differs by several factors such as wastewater sources [20,21] and the treatment methods of these waters [16]. The importance of this study is reinforced by the unique composition of Moroccan sewage sludge, which has not been studied in depth before. By providing detailed information on this specific type of sludge, our research contributes significantly to the optimization of pyrolysis processes adapted to variations in biomass composition, thus improving the feasibility and efficiency of waste-to-energy conversions. This literature will greatly encourage the industrial application of sludge pyrolysis through the optimization and design of adaptable and reliable pyrolysis plants for the valorization of this type of waste.

This study employs three isoconversion methods, namely KAS, FWO, and Starink. Advanced characterization techniques, including ultimate analysis, proximate analysis, infrared spectroscopy (FTIR), X-ray diffraction (XRD), differential scanning calorimetry (DSC), thermogravimetric analysis (TG-DTG), and thermal analysis-mass spectrometry (TA-MS), are utilized to provide a comprehensive understanding of the sludge's properties and behavior during pyrolysis. It provides crucial insights into the pyrolysis process and unveils the potential for waste valorization. This aligns with the broader goal of advancing sustainable practices in energy production and waste management, particularly in regions with similar sewage sludge characteristics.

2. Materials and Methods

2.1. Sample Preparation

Sludge samples were collected from the wastewater treatment plant in Benguerir (75 km from Marrakech city), a Moroccan town known for its phosphate mines. At the plant, the sewage sludge underwent biological treatment as part of the wastewater processing. After this biological treatment, the sludge was subjected to mechanical dehydration, resulting in a moisture content of approximately 79%. To further reduce this moisture content, the samples were then dried in an oven at 105 °C for 24 h. This drying process aimed to eliminate as much water as possible. The resulting dried sludge was manually ground using a mortar and pestle, sieved through a 100 µm sieve, and designated with the abbreviation SSB (Sewage Sludge of Benguerir).

2.2. Proximate, Ultimate, and HHV Analyses

Proximate analysis was carried out by the ASTM standard method (D5142-90) [22] using the thermogravimetric instrument NETZSCH STA 449F5. Ultimate analysis was performed using the elemental analyzer Thermo Scientific FlashSmart (Thermo Fisher

Scientific, Waltham, MA, USA). And to determine higher heating value HHV, a calorimetric bomb was used according to ASTM standard method (D2015-19) [23].

2.3. FTIR Analysis and X-ray Diffraction

The Fourier transform infrared FTIR analysis was achieved by the spectrometer THERMO IS50 FTIR system spectrum X (Thermo Fisher Scientific, Waltham, MA, USA) in the range 600–4000 cm^{-1} , with a total of 16 scans for each measurement. The X-ray diffraction analysis was performed with XRDynamic 500 diffractometer (Rigaku, Tokyo, Japan) with Cu-K α radiation ($\lambda = 1.54 \text{ nm}$) in a range of 5 and 70°.

2.4. TG-DTG, TG-MS, and DSC Analysis

The thermal behavior of the samples was studied through TG-DTG and DSC analysis, performed on an STA 449 F5 Jupiter Netzsch instrument (NETZSCH-Gerätebau GmbH, Selb, Germany). For TG-MS analysis, the QMS 403 Aeolos Quadro instrument (NETZSCH-Gerätebau GmbH, Germany) was utilized. The samples were placed in alumina crucibles and heated from room temperature to 1050 °C at three different rates (5, 10 and 20 K/min). Pyrolysis was performed under an argon flow of 50 mL/min and a shielding gas flow of 20 mL/min. The released gases were detected with the infrared spectrometer already connected to the instrument. To avoid condensation of the gaseous products for the TG-MS analysis, the transfer line of the TG balance head was heated to 250 °C.

2.5. Kinetic Study

The kinetic study of sewage sludge pyrolysis is essential to understand the evolution of the reaction and to determine the dependence of the rate of progression on the process parameters. It is generally carried out in two steps: the first step consists of experiments at different heating temperatures, and the second step is to determine mathematically the kinetic parameters such as the activation energy and the pre-exponential factor.

The second step is performed by mathematical methods which can be classified into three methods: model fitting, single heating rate, and iso-conversion, which are the most recommended compared to the other methods [24].

The transformation and decomposition of biomass during pyrolysis is described by Equation (1) [25]:

$$\frac{d\alpha}{dt} = \kappa(T)f(\alpha) \quad (1)$$

where,

$$\alpha = \frac{m_0 - m_t}{m_0 - m_r} \quad (2)$$

where, α is the conversion, m_0 is the initial weight of the sample, m_t is the weight of the sample at time t , and m_r is the weight of the residual of the sample during the process of pyrolysis.

Using the Arrhenius Equation (3), the TGA data can be analyzed:

$$\kappa(T) = A \exp\left(\frac{-E_a}{RT}\right) \quad (3)$$

where A is the pre-exponential coefficient (min^{-1}), E_a is the activation energy (J/mol), and R is the universal constant of perfect gases (8.314 J/mol.K)

By replacing the reaction rate with its formula (Equation (3)), Equation (1) becomes

$$\frac{d\alpha}{dt} = A \exp\left(\frac{-E_a}{RT}\right) f(\alpha) \quad (4)$$

where the term $f(\alpha)$ represents the conversion dependence of conversion and can be labeled as the “reaction model”. By introducing $\beta = dT/dt$ as the heating rate and integrating

Equation (4) for the initial conditions ($\alpha = 0$ at $T = T_0$) the integral form of the conversion rate will be:

$$g(\alpha) = \int_0^\alpha \frac{d\alpha}{f(\alpha)} = \frac{A}{\beta} \int_{T_0}^T \exp\left(\frac{-E_a}{RT}\right) dT = \frac{AE_a}{\beta R} p(x) \quad (5)$$

where $x = E_a/RT$. Equation (5) cannot be solved by analytical solutions, but approximate numerical methods can be used to solve it. In this work, the iso-conversional methods of FWO, KAS, and Starink have been used for the determination of E_a and A [24].

2.5.1. Activation Energy

The activation energy is the minimum energy needed to start a chemical reaction. As mentioned, the following methods are used to determine it.

(a) Flynn–Wall–Ozawa (FWO) method

The Flynn–Wall–Ozawa method estimates the temperature integral using the Doyle approximation [24]:

$$p(x) \cong \exp(-2.315 - 0.4567x) \quad (6)$$

Equation (6) applies the calculation of $p(x)$ for $x > 20$, and inserting the formula into Equation (5) gives:

$$\ln(\beta) = \ln\left(\frac{AE_a}{Rg(\alpha)}\right) - 5.331 - 1.052\left(\frac{E_a}{RT}\right) \quad (7)$$

Activation energy E_a can be calculated by evaluating the slope of $\ln(\beta)$ versus $1/T$ curves plotted for each value of α .

(b) Kissinger–Akahira–Sunose (KAS) method

The KAS equation uses the approximation given by Murray and White Equation (8), for the calculation of the temperature integral [24]:

$$p(x) \cong \frac{\exp(-x)}{x^2} \quad (8)$$

By replacing Equation (5) with Equation (8), and after simplifications, the KAS equation becomes [26]:

$$\ln\left(\frac{\beta}{T^2}\right) = \ln\left(\frac{AR}{E_a g(\alpha)}\right) - \frac{E_a}{RT} \quad (9)$$

The calculation of activation energy evaluated by the slope of versus $1/T$ curves plotted for each value of α .

(c) Starink method

The method developed by Starink allows obtaining the activation energy with more precision. Similar to the FWO and KAS methods, it is based on determining the slope as a function of $1/T$ for each value of α [24].

The Starink equation is given by the following formula:

$$\ln\left(\frac{\beta}{T^{1.92}}\right) = \ln\left(\frac{AR}{E_a g(\alpha)}\right) - 1.0008\left(\frac{E_a}{RT}\right) \quad (10)$$

2.5.2. Pre-Exponential Factor

The pre-exponential coefficient is related to the frequency of collisions between molecules (entropy) and the probability that these collisions lead to a reaction. It can

be derived from Kissinger's equation. The E_a values from the iso-conventional method can be substituted into Equation (11) to obtain the corresponding pre-exponential factor values:

$$A = \frac{\beta E_a \exp\left(\frac{E_a}{RT_m}\right)}{RT_m^2} \quad (11)$$

where T_m is DTG temperature peak (K).

2.5.3. Thermodynamic Parameters

Calculating thermodynamic data is important for defining process feasibility and performing energy calculations. Thermodynamic considerations are essential for understanding the changes in enthalpy (ΔH , kJ/mol), entropy (ΔS , kJ/mol.K), and free energy (ΔG , kJ/mol) in transformations. These parameters were calculated using the following formulas [24]:

$$\Delta H = E_a - RT \quad (12)$$

$$\Delta G = E_a + RT_m \ln\left(\frac{K_B T_m}{hA}\right) \quad (13)$$

$$\Delta S = \frac{\Delta H - \Delta G}{T_m} \quad (14)$$

where, K_B is Boltzmann constant ($1.38064852 \times 10^{-23}$ J.K⁻¹) and h is Plank's constant ($6.62607004 \times 10^{-34}$ J.s).

3. Results and Discussion

3.1. Proximate, Ultimate, and HHV Analysis

To determine the chemical characteristics of the sewage sludge, proximate and ultimate analyses were performed on SSB by external calibration using two high-purity organic compounds: methionine (C₅H₁₁NO₂S) and BBOT (2,5-Bis(5-tert-butyl-2-benzoxazol-2-yl)thiophene, C₂₆H₂₂N₂O₂S). The objective of the proximate analysis is to determine the moisture content (M), volatile matter (VM), fixed carbon (FC), and ash content of the sewage sludge. The ultimate analysis aims to determine the content of Nitrogen (N), Carbon (C), Hydrogen (H), Sulfur (S), and Oxygen (O) of the samples [27].

The main results obtained were summarized in Table 1 and compared with results found in the literature [28–30].

Table 1. Ultimate and proximate analyses of sewage sludge.

	Sample	Ultimate Analyses						Proximate Analyses				
		N (wt.% db)	C (wt.% db)	H (wt.% db)	S (wt.% db)	O (wt.% db)	M (wt.%)	VM (wt.%)	FC (wt.%)	Ash (wt.%)	HHV (MJ/kg) Experimented	HHV (MJ/kg) Estimated
Present work	SSB (methionine)	3.93	33.55	4.44	1.36	18.74	2.44	48.54	11.04	37.98	15.16	14.282
	SSB (BBOT)	3.86	33.55	4.49	1.39	18.75	2.44	48.54	11.06	37.96	15.01	14.344
Previous work	Sewage sludge [28]	4.1–5.3	28.9–32.3	4.4–4.9	0.57–1.1	20.2–24.9	4.2–19.1	63.5–64.9	-	32–36.2	-	12.24–13.12
	Sewage sludge [29]	2.9–5.78	25.39–38.2	4.06–6.19	0.77–1.17	20.84–22.08	4.3–6.8	53.1–64.9	2.1–7.9	27.2–44.8	-	11.84–17.75
	Rice straw [30]	0.87	38.24	5.20	0.18	36.26	-	65.47	15.86	18.67	15.09	-

db: dry basis.

The moisture content, volatile matter, and ash content were obtained from the TG analysis curves performed in inert and oxidizing media, and the fixed carbon content was calculated using Formula (15).

$$FC = 100 - M - VM - Ash \quad (15)$$

According to the results obtained in Table 1, the SSB have a lower volatile matter rate (48%) and a higher fixed carbon rate (11%) than those found in sewage sludge from previous works [28,29]. This difference is due to several factors such as the activity of the area from which the water comes, and the treatments used in the wastewater treatment plant. Concerning the ash content, it reaches an average value of 37.97%, which is a very high value compared to other types of biomasses such as rice straw [30].

For the ultimate analysis results, the sludge contains a very high amount of carbon and oxygen (33.5 and 18.7%) and a low amount of nitrogen, hydrogen, and sulfur (3.9, 4.4, and 1.3%). The rates of organic elements found in SSB are within the ranges found in previous investigation [28,29].

The correlation developed by Channiwala and Parikh (2002) [31] is used for the estimation of the higher heating value (HHV) since the rate of elements is in the range $0\% \leq C \leq 92.25\%$, $0\% \leq H \leq 25.15\%$, $0\% \leq O \leq 50\%$, $0\% \leq N \leq 5.6\%$, $0\% \leq S \leq 94.08\%$, $0\% \leq Ash \leq 71.4\%$.

$$HHV = 0.3491C + 1.1783H + 0.1005S - 0.1034O - 0.0151N - 0.0211Ash \quad (16)$$

For more accuracy, a bomb calorimeter was used to determine the HHV according to the ASTM standard method (D2015-19), and the results show higher values than that estimated with Equation (16) (15.085 MJ/kg against 14.31 MJ/kg, average value). The SSB's HHV is similar to that of rice straw which has proven, after its pyrolysis, that it has energy potential [32], which encourages energy conversion of sewage sludge.

3.2. FTIR Analysis and X-ray Diffraction

The objective of the infrared spectroscopic analysis is to determine the chemical composition of the sewage sludge. Figure 1 shows the spectrum obtained from the FTIR analysis.

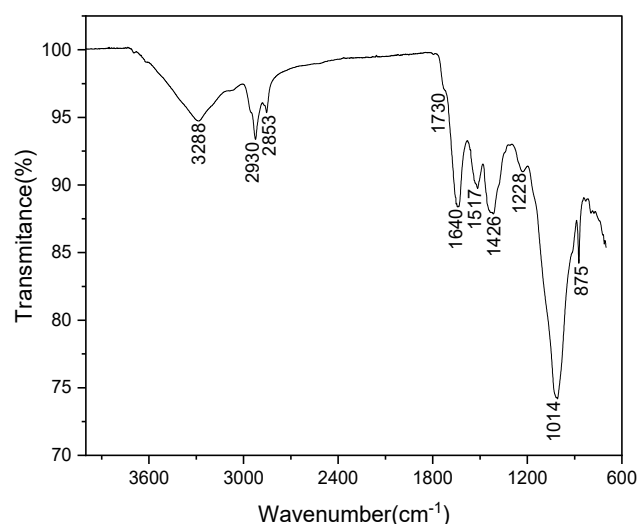


Figure 1. Infrared spectrum of SSB.

The broad peak 3288 cm^{-1} was a stretching vibration of the -OH surface association that also appeared at the 1640 peak [33]. This association structure resulted in many hydrogen bonds in the sewage sludge. It prevents the release of H_2O during the drying

process and maintains the structure. The stretching vibration that was related to the prominent absorption peak at 2930 and 2853 shows the existence of C-H in aliphatic [34,35].

The stretching region of double bonds, such as N=H and C=O, is found between 2000 and 1500 cm^{-1} [36]. The stretching vibrations of CaCO_3 are indicated by peaks at 1426 and 875 cm^{-1} [37,38]. Additionally, the peaks that appear between 1000 and 840 cm^{-1} correspond to C-O stretching vibrations in polysaccharides and Si-O bond stretching vibrations in silicates [35]. These could also be associated with vibrations from P-O-P and P-O bonds, especially considering that the sludge was sourced from an area with a prevalent phosphate mining industry.

To identify the crystalline phases and surface functional groups of SSB, an X-ray diffraction analysis was performed, and the results are presented in Figure 2.

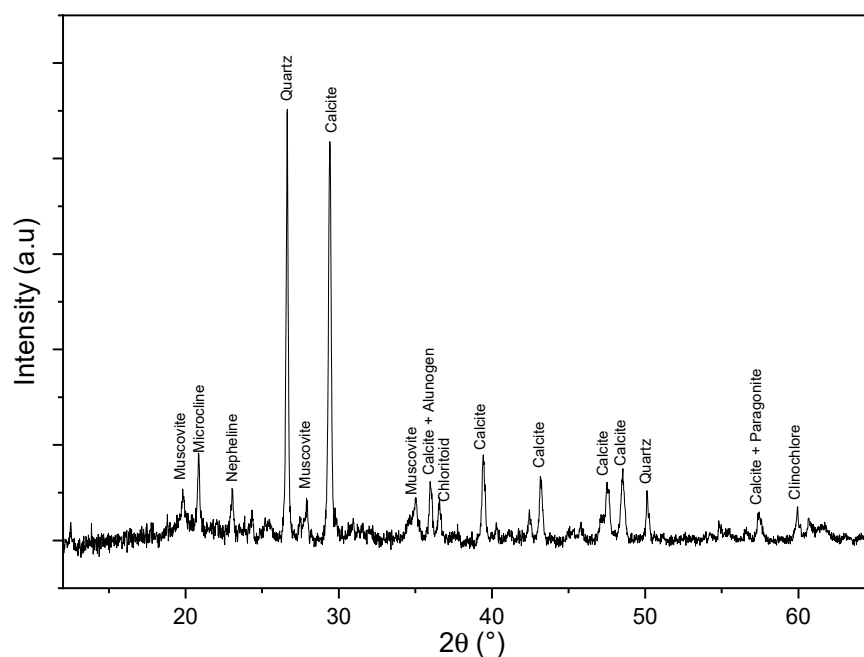


Figure 2. X-ray diffraction patterns of SSB.

The main peaks found in the XRD spectrum are muscovite, microcline, nepheline, quartz, calcite, alunogen, chloritoid, paragonite, and clinocllore minerals, noting that quartz and calcite are the most dominant in the SSBs. These minerals contain alkali metals such as Na, K, Mg, and Ca, metalloids such as Al and Si, and transition metals such as Fe.

3.3. TG-DTG, TG-MS, and DSC Analysis

The curves of the thermogravimetric analysis (TG) and (DTG) of the SSB for the three heating rates during the pyrolysis process are shown in Figure 3. According to the results, the pyrolysis of the SSB can be distinguished into four stages. The first stage occurs in the temperature range 0–150 °C with a loss of mass not exceeding 1.8% for the three heating rates; it is the preheating phase which corresponds to the loss of water and a small amount of volatile substances [39,40]. The second stage is where the degradation of the organic matter begins as the decomposition of hemicellulose and cellulose compounds [41]; it is located in the temperature range 150–560 °C where the degradation of the mass reaches an average value of 48% for the three-heating speeds. The two types of organic matter degradation that occurred during this stage are the degradation of lipids and carbohydrates between 150 and 400 °C and the decomposition of proteins between 400 and 560 °C [40].

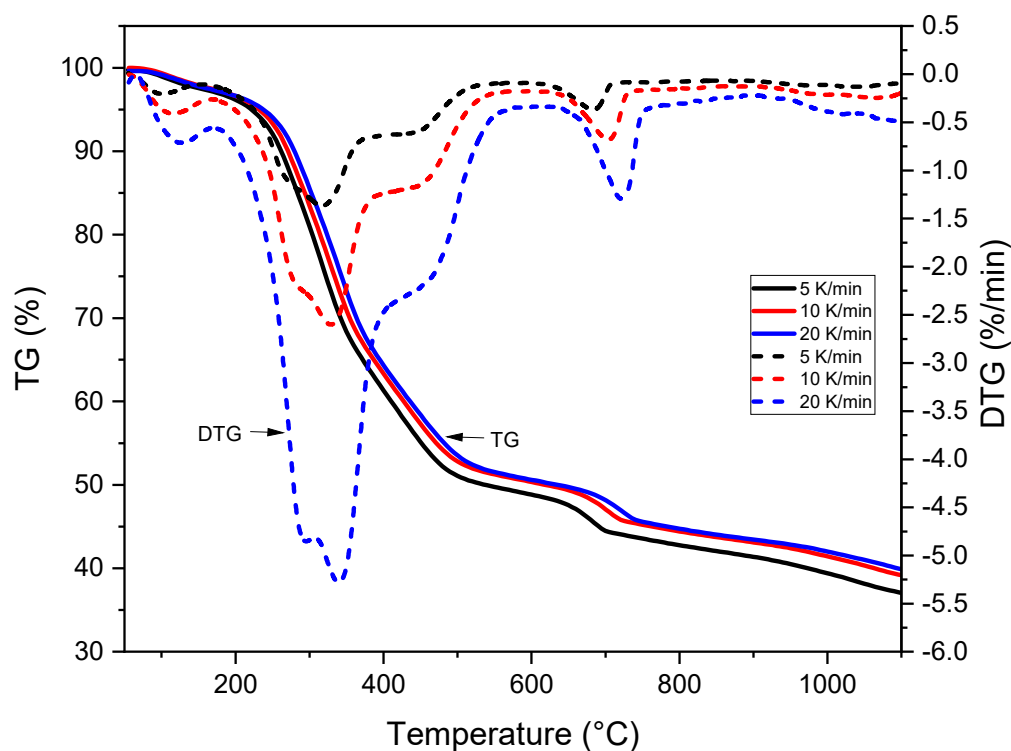


Figure 3. The TG and DTG curves of SSB at different heating rates.

In the third stage, which occupies the temperature range 560–900 °C, the mass loss becomes slow, about 7%, and this is mainly due to the decomposition of the calcium carbonate as shown by the DTG peaks between 680 and 725 °C of the dry sludge [29]. Further confirmation of the presence of calcium carbonate in the SSB comes from the X-ray diffraction analysis already carried out as calcite. After 900 °C, the fourth stage arrives where lignin decomposition can continue even though its existence is low in sewage sludge [42,43] but its pyrolysis is a slow process that occupies a wide temperature range [36,42,44].

Regarding the influence of the heating rate on the TG-DTG analysis, as the curves show (Figure 3), with the increase of its speed, the peaks of mass loss move towards the region of the high temperatures, the intensity of the peaks becomes wider, and the loss of mass increases. This can be explained by the difficulty in accurately measuring the temperature of the sample due to the increase in the temperature gradient between the surface and the interior of the solid, noting that the temperature gradient increases with the heating rate, resulting in the shift of the curves towards the high temperature region [35]. Also, when the sample undergoes chemical reactions in a temperature region, the reaction depends strongly on the heating rate, therefore, the higher the heating rate the more the reactions move to higher temperatures [45].

The literature describes that a higher heating rate increases the production of volatiles (governed by chemical reactions) and favors the retention of volatiles (controlled by diffusion). So, the chemical events occurring result from a competition between the kinetics of the formation of volatiles and their diffusion [46].

This can also be explained by the influence of the heating rate on the reaction residence time. The lower the heating rate, the slower the reaction residence time, therefore, the degradation of the substrate ends in lower temperatures [47].

The results of TG-MS analysis are presented in Figure 4a–f. This analysis allows for the following of the gas emissions produced by the SSB degradation during the pyrolysis process.

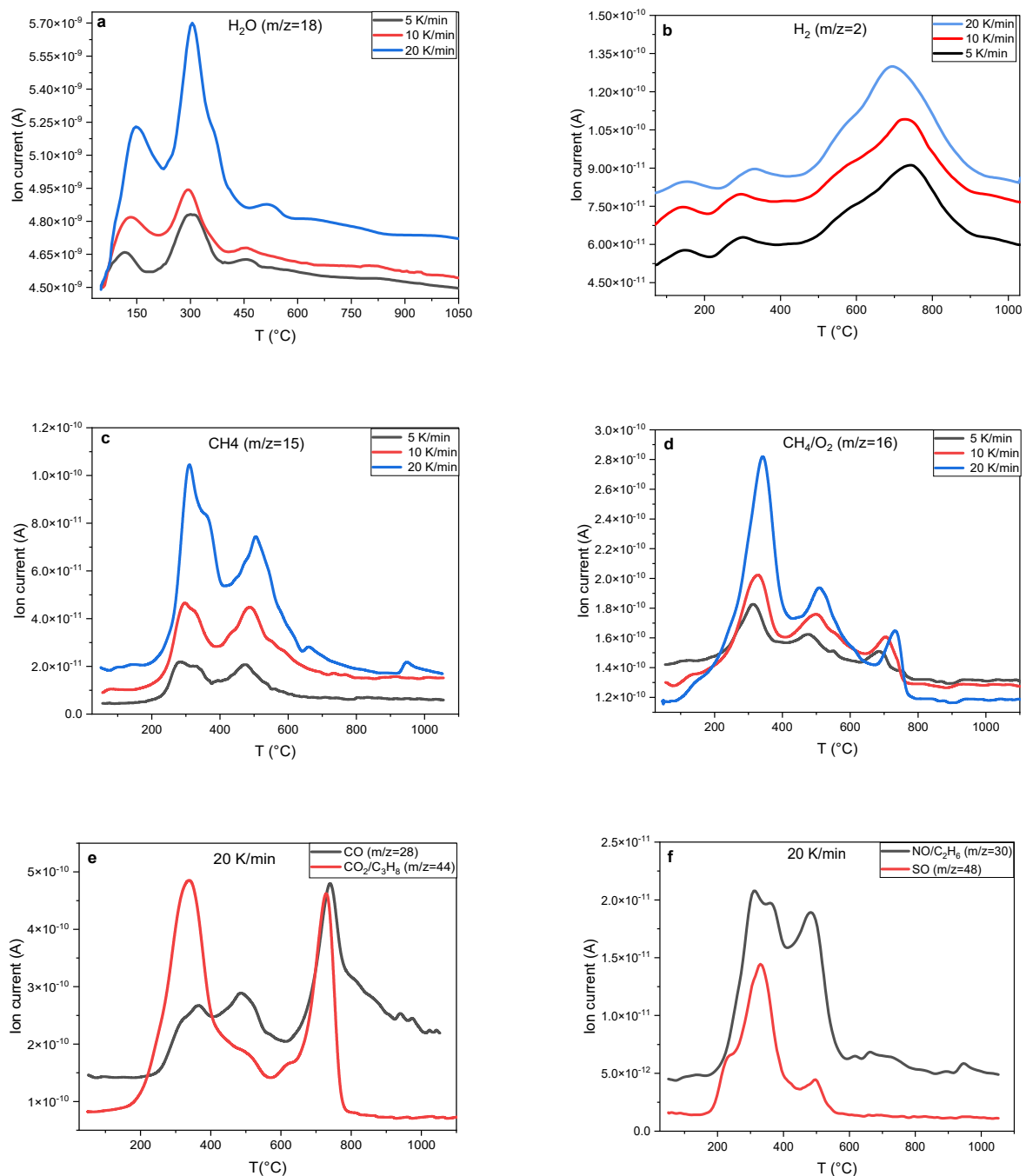


Figure 4. Gas evolution during SSB pyrolysis, (a) $m/z = 18$, (b) $m/z = 2$, (c) $m/z = 15$, (d) $m/z = 16$, (e) $m/z = 28$ and 44, (f) $m/z = 30$ and 48.

The mass spectrum of the water molecule ($m/z = 18$) in Figure 4a was detected in two temperature ranges:

From 0 to 200 °C, where the sludge is dewatered, and the water molecules are released by evaporation;

From 200 °C to 400 °C, where the pyrolysis phase occurs and the crystalline water is decomposed [48]. The highest H_2O production is detected at 300 °C.

The H_2 molecule ($m/z = 2$) occurs in three temperature regions according to Figure 4b. The first two regions are the regions where drying and degradation of organic matter take place, and this is due to the release of H_2O as already shown in Figure 4a. The main H_2 production between 600 and 900 °C is issued from the loss of aromatic CH groups and

heterocyclic compounds [48,49]. The intensity of the H₂ peak increases at 500 °C, which corresponds to the beginning of the third phase of pyrolysis.

The spectra corresponding to methane CH₄ ($m/z = 15$ and 16) in Figure 4c,d occupies the temperature region between 200 and 600 °C. The emission of methane comes from the decomposition of organic matter that occupies phase II of pyrolysis, as mentioned in the section of TG-DTG analyses, and it was detected to have its maximum release at the temperature 300 °C. Another peak was observed for ($m/z = 16$) between 680 °C and 730 °C. This peak can be related to the release of O₂ from the calcination of calcium carbonate CaCO₃ performed with the following chemical equation:



CO₂ can decompose and give (CO + O), explaining the appearance of the peak between 680 and 730 °C.

It can be noted that the intensity of the peaks of the spectra increases with the increase of the heating rate and that the curves move towards the higher temperatures. This can be explained by the fact that the gradient of temperature increases when the heating rate increases and the explanation is the same as for the displacement of the TGA-DTG curves. However, for the three heating speeds (5, 10, and 20 K/min), the gas emissions are similar in the same temperature regions. In the spectra of ($m/z = 28, 30, 44,$ and 48), only the curves obtained at the 20 K/min heating rate were presented.

Figure 4e depicts the spectrum of ($m/z = 28$) CO gas and ($m/z = 44$) CO₂ gas or C₃H₈ gas. The emissions of these gases cover the temperature region between 150 and 800 °C. The second phase of pyrolysis takes place between 150 and 600 °C, during which the organic matter decomposes, and thus releases CO and CO₂. It is noted that the intensity of CO₂ at 300 °C is greater than that of CO, knowing that there is no oxygen present in the pyrolysis process. Therefore, the peak may present the C₃H₈ or the CO₂, explaining the increase of the peak at the temperature of 300 °C compared to the peak of CO at the same temperature.

Normally the release of CO and CO₂ decreases with increasing temperature [50], which is not validated in this case. The intensity of the CO and CO₂ peaks increased between 600 and 800 °C. This can be explained by the fact that calcium carbonate degrades in this temperature region as already mentioned in the TG-DTG analysis, thus the emission of CO₂, which decomposes itself and gives CO with such an intense peak, confirm the appearance of O already in Figure 4d.

Figure 4f presents two spectra, the first of which corresponds to ($m/z = 30$) which may be C₂H₆ or NO gas, and the second corresponds to ($m/z = 48$) which may be SO related. There is a high probability of NO and SO gas release because the SSB showed the presence of nitrogen and sulfur from the ultimate analysis. Both gases are released during the second phase of pyrolysis. Additional analysis and testing are important to increase the certainty and determine if the amount of harmful gases produced complies with environmental regulations as the TG-MS gas analysis is insufficient to quantify these products.

DSC calorimetry is a thermal analysis technique that measures the differences in heat exchange between the sample under the test and a reference. Figure 5 shows the results of SSB differential scanning calorimetry during pyrolysis. As shown in the figure, three main endothermic reactions appear. The first reaction occurs between 0 °C and 150 °C, indicating the evaporation of water from the sewage sludge. The second reaction occurs between 200 °C and 560 °C and has three distinct peaks, indicating the decomposition of the organic matter. The last reaction presents a large and intense peak between 600 °C and 800 °C, showing the decomposition of the calcium carbonate. These results confirm what was found in the TG-DTG results.

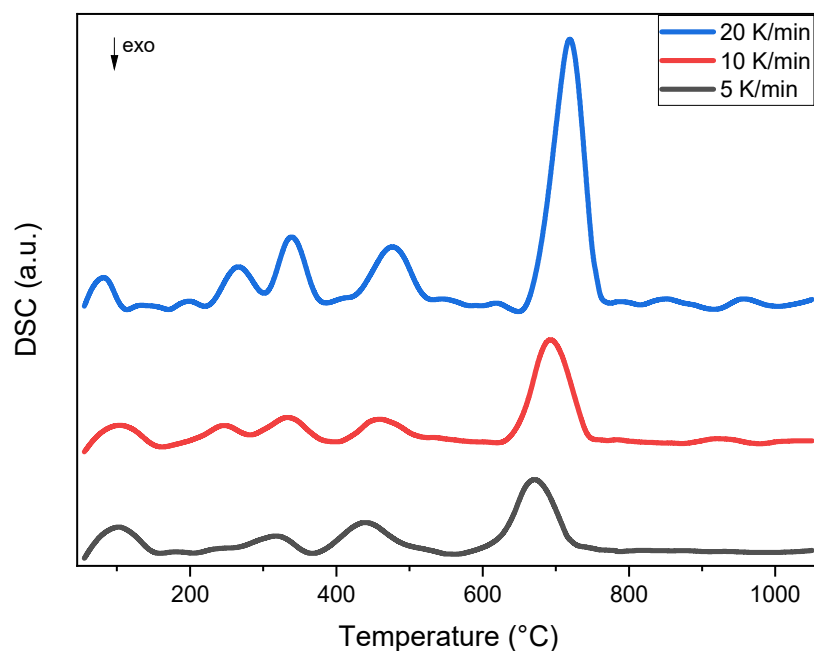


Figure 5. DSC curves of SSB during pyrolysis.

3.4. Kinetic Study

3.4.1. The Activation Energy

In this study three isoconversional methods were used with three heating rates (5, 10, and 20 K/min) for the calculation of kinetic parameters of SSB pyrolysis. It can be noted that the isoconversional methods are the methods recommended by the International Confederation of Thermal Analysis and Calorimetry (ICTAC) [51] in 2011 and 2014 for the determination of kinetic parameters.

Figure 6 shows the linear fit for the three isoconversional methods: FWO, KAS, and Starink for different conversion rates ranging from 0.1 to 0.9 with a step size of 0.1. The determination of the straight-line slopes from Figure 6 allows the calculation of the activation energy as summarized in Table 2.

Table 2. Activation energies E_a and coefficient of determination R^2 versus conversion rate α for SSB.

α	KAS Method		FWO Method		Starink Method	
	E_a (kJ/mol)	R^2	E_a (kJ/mol)	R^2	E_a (kJ/mol)	R^2
0.1	175.4	0.953	200.0	0.985	166.9	0.944
0.2	209.2	0.979	201.9	0.975	202.5	0.976
0.3	228.5	0.979	222.1	0.976	222.6	0.976
0.4	191.1	0.998	182.6	0.998	183.2	0.998
0.5	258.4	0.954	253.3	0.947	253.9	0.948
0.6	443.4	0.997	447.7	0.997	448.1	0.997
0.7	810.8	0.856	833.7	0.850	833.8	0.85
0.8	953.3	0.856	983.1	0.851	983.1	0.851
0.9	450.9	0.915	451.9	0.907	452.5	0.907
Average	413.4	0.946	419.6	0.947	416.3	0.938

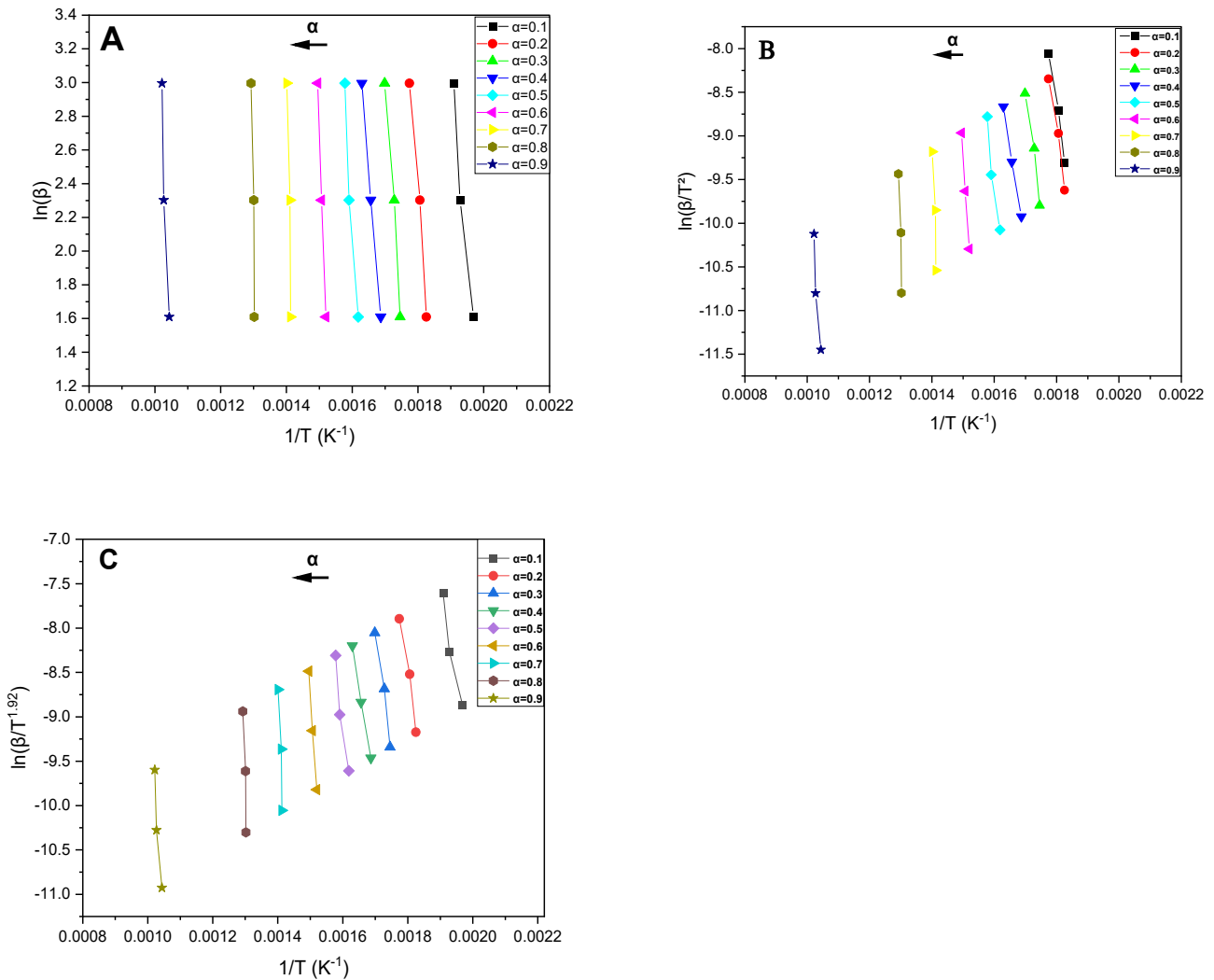


Figure 6. Graphical representation of FWO (A), KAS (B), and Starink (C).

The results of the activation energy from Table 2 are presented in Figure 7. The graphical representation shows that there is not a big difference between the E_a calculated by the three methods KAS, FWO, and Starink. It can be noted that E_a increases with the increase of conversion rate until reaching the maximum value at $\alpha = 0.8$, then it decreases for the three models. The increase is due to the decomposition of lignin which needs higher energy than the one necessary for the decomposition of cellulose and hemicellulose [52]. However, it should be noted that sewage sludge is composed of various constituents other than cellulose, lignin, and hemicellulose which make up the majority of biomass [53]. Furthermore, the decrease can be attributed to a shift in the pyrolysis reaction mechanism. As the process progresses, the decomposition of simpler or already partially degraded materials becomes dominant, requiring less energy compared to the initial stages where complex polymers like lignin are decomposed.

The coefficient of determination R^2 is almost the same for the three isoconversional methods. It reaches values (>0.95) for a conversion rate (<0.7), with a maximum value at $\alpha = 0.6$, therefore the values of the activation energy are more accurate for the lower conversion rate.

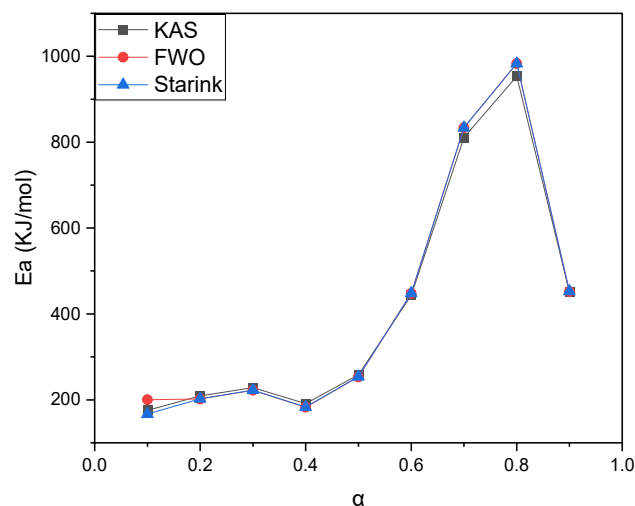


Figure 7. Activation energy of pyrolysis process of SSB using KAS, FWO, and Starink methods.

For the FWO, KAS, and Starink models, E_a values range between 182.6–983.1 kJ/mol, 175.4–953.3 kJ/mol, and 166.9–983.1 kJ/mol, respectively. They are higher than those calculated in Shahbeig and Nosrati's (2020) [13] work, who found values between 59.3–247.4 kJ/mol, 52.2–235.4 kJ/mol, and 52.3–235.9 kJ/mol using the FWO, KAS, and Starink methods respectively. This was also observed in Naqvi et al.'s (2018) [17] work which determined the values of Friedman (10.6–306.2 kJ/mol), FWO (45.6–231.7 kJ/mol), KAS (41.4–232.1 kJ/mol), and Popescu (44.1–241.1 kJ/mol) accordingly.

The high E_a values in this study are recorded at conversion rates ($\alpha > 0.7$), where complex reactions occur, such as the decomposition of lignin and the calcination of calcium carbonate. The CaCO_3 , in particular, may require significantly high activation energies [54,55], which explains the elevated values observed in this study.

3.4.2. The Pre-Exponential Factor

The pre-exponential factor is determined by Equation (11) using the activation energy calculated by the KAS, FWO, and Starink methods. The results are grouped in Table 3.

The results indicate that the factor A increases with the conversion rate. The point that validates the calculated results of the activation energy is that the higher the pre-exponential the more energy the reaction requires to start, therefore E_a is also higher.

The factor A describes the solid phase chemistry of the reaction, which is directly related to the structure of the material and is crucial to optimize the pyrolysis of the biomass. The calculated values of A are between 1.40×10^{16} and $5.13 \times 10^{86} \text{ min}^{-1}$, 1.98×10^{18} and $2.32 \times 10^{89} \text{ min}^{-1}$, and 2.51×10^{15} and $2.32 \times 10^{89} \text{ min}^{-1}$ with KAS, FWO, and Starink methods, respectively. The three range values are $>10^{10} \text{ min}^{-1}$ which reflects the complex nature of the sample and the complexity of the reaction during the decomposition of the material [56].

The pre-exponential factor was evaluated using the compensation factor approach. The approach assumes that a linear relationship will exist between E_a and A if their values differ very significantly with each reaction model.

The compensation factor approach observed for the KAS, FWO, and Starink methods is presented in Figure 8. The presentation of $\ln(A)$ as a function of E_a is expressed as

$$\ln(A_i) = a + bE_{ai} \quad (18)$$

with i is the heating rate (5, 10, and 20 K/min).

Table 3. The pre-exponential coefficient for different heating rates of SSB.

α	Pre-Exponential Coefficient A (min^{-1})								
	KAS Method			FWO Method			Starink Method		
	5 K/min	10 K/min	20 K/min	5 K/min	10 K/min	20 K/min	5 K/min	10 K/min	20 K/min
0.1	6.66×10^{16}	2.79×10^{16}	1.40×10^{16}	1.17×10^{19}	4.35×10^{18}	1.98×10^{18}	1.11×10^{16}	4.83×10^{15}	2.51×10^{15}
0.2	8.05×10^{19}	2.87×10^{19}	1.26×10^{19}	1.75×10^{19}	6.43×10^{18}	2.91×10^{18}	1.96×10^{19}	7.21×10^{18}	3.26×10^{18}
0.3	4.50×10^{21}	1.46×10^{21}	5.95×10^{20}	1.19×10^{21}	3.99×10^{20}	1.67×10^{20}	1.34×10^{21}	4.46×10^{20}	1.86×10^{20}
0.4	1.78×10^{18}	6.91×10^{17}	3.26×10^{17}	3.05×10^{17}	1.23×10^{17}	6.01×10^{16}	3.44×10^{17}	1.39×10^{17}	6.75×10^{16}
0.5	2.32×10^{24}	6.53×10^{23}	2.37×10^{23}	8.14×10^{23}	2.34×10^{23}	8.66×10^{22}	9.08×10^{23}	2.61×10^{23}	9.63×10^{22}
0.6	1.11×10^{41}	1.29×10^{40}	2.27×10^{39}	2.72×10^{41}	3.08×10^{40}	5.33×10^{39}	2.94×10^{41}	3.33×10^{40}	5.75×10^{39}
0.7	9.22×10^{73}	1.83×10^{72}	7.67×10^{70}	1.04×10^{76}	1.86×10^{74}	7.10×10^{72}	1.06×10^{76}	1.89×10^{74}	7.24×10^{72}
0.8	5.13×10^{86}	5.14×10^{84}	1.23×10^{83}	2.32×10^{89}	2.02×10^{87}	4.31×10^{85}	2.32×10^{89}	2.02×10^{87}	4.31×10^{85}
0.9	5.28×10^{41}	5.89×10^{40}	1.01×10^{40}	6.52×10^{41}	7.25×10^{40}	1.23×10^{40}	7.28×10^{41}	8.08×10^{40}	1.37×10^{40}

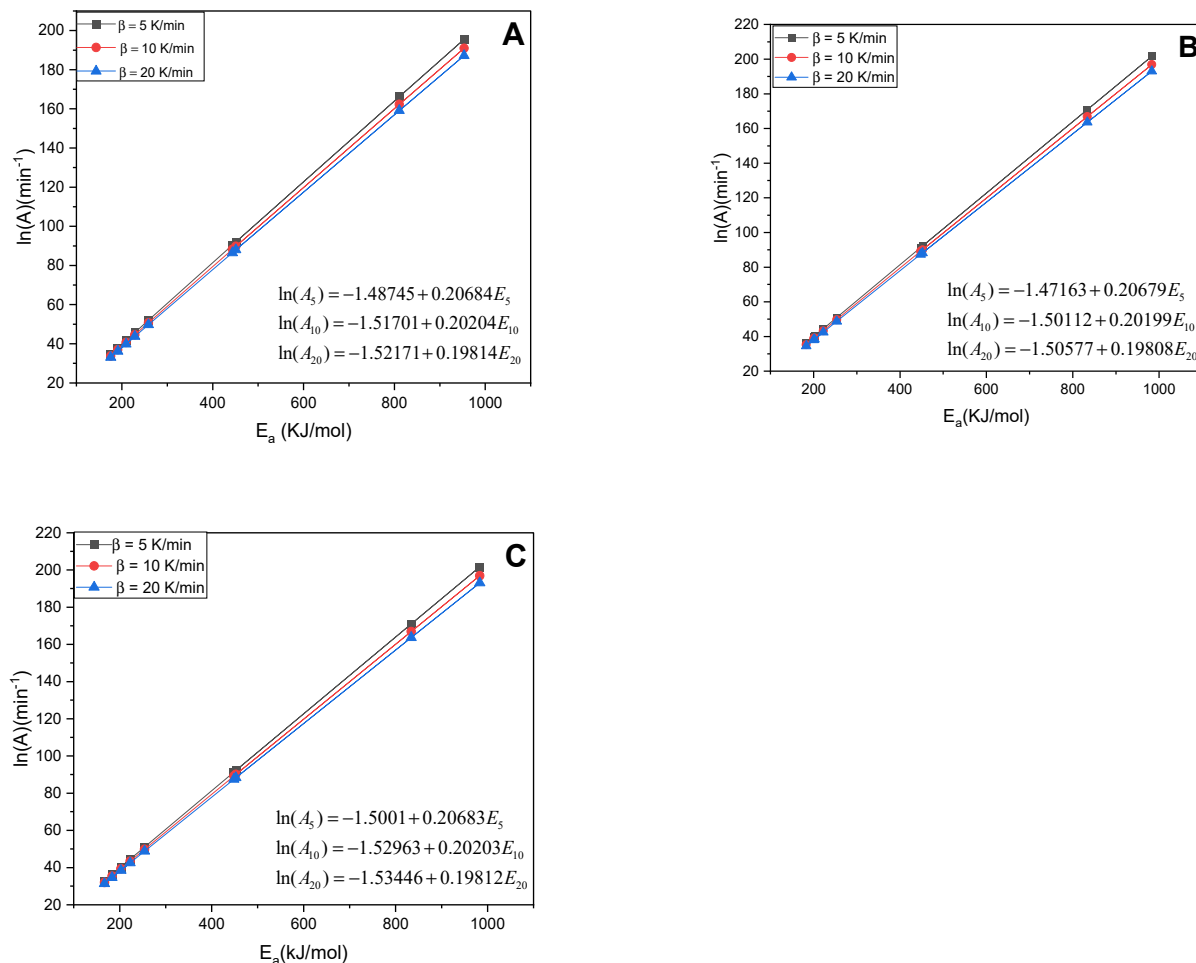


Figure 8. Linear fit plots of the SSB’s compensation technique for the KAS (A), FWO (B), and Starink (C) models.

The R^2 for all equations presented in Figure 8 are of order 1, which gives an excellent linear relationship between $\ln(A)$ and E_a .

3.4.3. Thermodynamic Parameters

Equations (12)–(14) have been used to calculate the thermodynamic parameters, which are listed in the Table 4.

Table 4. Thermodynamic parameters of SSB using FWO, KAS, and Starink methods.

α	β (K/min)	KAS Method			FWO Method			Starink Method		
		ΔH (kJ/mol)	ΔG (kJ/mol)	ΔS (kJ/mol.K)	ΔH (kJ/mol)	ΔG (kJ/mol)	ΔS (kJ/mol.K)	ΔH (kJ/mol)	ΔG (kJ/mol)	ΔS (kJ/mol.K)
0.1	5	171.198	153.401	0.030	195.811	152.759	0.073	162.680	153.644	0.015
	10	171.108	157.348	0.022	195.721	156.691	0.064	162.590	157.597	0.008
	20	171.066	160.611	0.017	195.679	159.941	0.058	162.549	160.865	0.003
0.2	5	204.680	152.539	0.088	197.386	152.713	0.076	197.945	152.700	0.077
	10	204.632	156.466	0.080	197.338	156.644	0.067	197.896	156.630	0.069
	20	204.548	159.711	0.073	197.254	159.892	0.060	197.813	159.879	0.062
0.3	5	223.700	152.110	0.121	217.346	152.248	0.110	217.890	152.236	0.112
	10	223.652	156.026	0.112	217.298	156.167	0.101	217.841	156.156	0.103
	20	223.569	159.263	0.104	217.215	159.407	0.094	217.758	159.395	0.095

Table 4. Cont.

α	β (K/min)	KAS Method			FWO Method			Starink Method		
		ΔH (kJ/mol)	ΔG (kJ/mol)	ΔS (kJ/mol.K)	ΔH (kJ/mol)	ΔG (kJ/mol)	ΔS (kJ/mol.K)	ΔH (kJ/mol)	ΔG (kJ/mol)	ΔS (kJ/mol.K)
0.4	5	186.121	152.984	0.056	177.724	153.203	0.041	178.306	153.188	0.043
	10	186.031	156.921	0.048	177.634	157.146	0.034	178.215	157.130	0.035
	20	185.948	160.175	0.041	177.551	160.405	0.027	178.132	160.389	0.029
0.5	5	253.241	151.509	0.173	248.214	151.605	0.164	248.744	151.595	0.165
	10	253.151	155.411	0.162	248.124	155.509	0.153	248.654	155.499	0.155
	20	253.109	158.635	0.153	248.082	158.735	0.145	248.612	158.725	0.146
0.6	5	437.930	148.870	0.491	442.236	148.823	0.499	442.620	148.819	0.500
	10	437.881	152.709	0.473	442.187	152.660	0.481	442.572	152.657	0.482
	20	437.840	155.879	0.459	442.146	155.830	0.466	442.530	155.826	0.467
0.7	5	804.882	145.921	1.121	827.844	145.785	1.160	827.939	145.785	1.161
	10	804.875	149.689	1.088	827.837	149.550	1.127	827.932	149.550	1.127
	20	804.833	152.800	1.062	827.795	152.657	1.100	827.891	152.657	1.100
0.8	5	946.972	145.130	1.364	976.693	144.980	1.415	976.699	144.980	1.415
	10	946.965	148.879	1.326	976.686	148.725	1.375	976.692	148.726	1.376
	20	946.924	151.973	1.295	976.645	151.816	1.343	976.650	151.817	1.344
0.9	5	442.949	148.788	0.500	443.978	148.777	0.502	444.512	148.772	0.503
	10	442.818	152.625	0.482	443.847	152.613	0.483	444.380	152.608	0.485
	20	442.776	155.794	0.467	443.805	155.782	0.469	444.339	155.776	0.470

The enthalpy is the sum of the available internal energy of the biomass. Its variation with the variation of conversion rate α expresses the amount of energy consumed by the raw material during pyrolysis for its transformation during pyrolysis. The values of ΔH vary between 171.066 and 946.972 kJ/mol, 177.551 and 976.693 kJ/mol, and 162.549 and 976.699 kJ/mol for the kinetic methods KAS, FWO, and Starink, respectively. The values of ΔH are all positive because the reaction of pyrolysis is endothermic. This confirms the results found in the DSC analysis. Also, there is a difference about 5 kJ/mol between the values of E_a and ΔH . This indicates the formation of products during the reaction is favored by a lower potent energy [57]. Moreover, the values of ΔH are consistent with the values of E_a and A which shows the reliability of the data.

The maximum amount of mechanical effort that can be produced from a given amount of a certain substance is called Gibbs free energy. As the reaction progresses, the change in the available energy of the system is represented by the difference in the free energy values (ΔG). It can be observed from the table that ΔG values are all positive which are, on average, 153.784, 153.743, and 153.837 KJ/mol for KAS, FWO, and Starink methods, respectively.

In Table 4, the calculated values of ΔS (entropy variation) are all positive indicating higher disorder of products than reactants by dissociation of liaison [14] sewage sludge during slow pyrolysis. Since the Gibbs energy values are also positive, it means that the chemical reaction is spontaneous in the high temperatures or in the opposite direction. This conclusion is different from those found in the work of Naqvi et al. (2018) [17] and Shahbeig and Nosrati (2020) [13], who observed that during the pyrolysis of sewage sludge, the chemical reaction is not spontaneous. This difference can be explained by the higher activation energy values found in this work compared to those found in previous works. The reason is linked to high values of ΔH which induces a positive value of the difference between ΔH and ΔG . This is due to the complexity of the composition of sludge, especially because biomass can take a different form of chemical composition depending on the source of the wastewater and the activity of the area where it comes from. It is also remarkable that ΔS values vary in a wide range (0.003 and 1.415 KJ/mol.K) which confirms the complexity of the reaction of the sludge during pyrolysis.

4. Conclusions

The pyrolysis of the sludge from the wastewater treatment plant is carried out after its physicochemical characterization with the help of proximate analysis, ultimate analysis, FTIR, and XRD. The investigation showed that the sludge is generally composed of organic matter with a high rate of volatile matter and ashes, as well as an important HHV with a value of 15 MJ/kg.

The behavior of the sludge during pyrolysis is divided into 4 stages as determined by TG-DTG analyses; the first and second are devoted to drying and degradation of organic matter, while the third corresponds mainly to the beginning of calcium carbonate decomposition, and the last stage to the inorganic matter decomposition at high temperature. The TG-MS analysis showed the release of several gases such as H₂O, H₂, CH₄, O₂, CO₂, C₃H₈, CO, NO, and SO. The thermokinetic study was carried out using three isoconversional methods: KAS, FWO, and Starink. The values calculated from these methods are almost the same and the activation energy reaches very high values compared to the literature results. A positive ΔG and a positive ΔS showed that the chemical reaction during the pyrolysis is spontaneous at high temperatures or in the opposite direction. This is related to the complexity of the sludge chemical composition studied in this work.

The results of the study are essential for improving the modeling of the pyrolysis process. This will not only improve process efficiency, but also contribute to the advancement of pyrolysis technologies in the field of waste management. The application of this knowledge offers significant potential in optimizing the use of sewage sludge, underlining the practical relevance of this research.

Author Contributions: Conceptualization, H.M. and A.K.; Methodology, H.M. and A.K.; Formal analysis, H.M., A.K., and I.B.; Investigation, H.M., A.K., and M.A.; Data curation, H.M.; Writing—original draft, H.M. and A.K.; Writing—review and editing; H.M., A.K., I.B., M.A., S.B., T.B., B.S., and A.R.; Visualization, H.M.; Validation, I.B. and M.A.; Resources, I.B., S.B., and E.G.B.; Supervision, M.A. All authors have read and agreed to the published version of the manuscript.

Funding: This research received no external funding.

Data Availability Statement: Data are contained within the article.

Acknowledgments: This study was financially supported by the Green Energy Park. The authors are very appreciative of their support and the opportunity to work on their research platform.

Conflicts of Interest: The authors declare that they have no known competing financial interests or personal relationships that could have appeared to influence the work reported in this paper.

References

1. Rijksdienst voor Ondernemend Nederland. Business Opportunities Report for Reuse of Wastewater in Morocco Commissioned by the Netherlands Enterprise Agency. 2018. Available online: <https://www.rvo.nl/sites/default/files/2018/06/Business-opportunities-report-for-reuse-of-wastewater-in-morocco.pdf> (accessed on 13 September 2023).
2. Fijalkowski, K.; Rorat, A.; Grobelak, A.; Kacprzak, M.J. The presence of contaminations in sewage sludge—The current situation. *J. Environ. Manag.* **2017**, *203*, 1126–1136. [[CrossRef](#)]
3. Seggiani, M.; Puccini, M.; Raggio, G.; Vitolo, S. Effect of sewage sludge content on gas quality and solid residues produced by cogasification in an updraft gasifier. *Waste Manag.* **2012**, *32*, 1826–1834. [[CrossRef](#)]
4. Zerrouqi, Z.; Sbaa, M.; Chafi, A.; Elhafid, D. Investigation du lessivage des stocks de boues d'épuration de Nador: Étude sur terrain et apport de l'expérimentation. *J. Water Sci.* **2012**, *24*, 371–381. [[CrossRef](#)]
5. Oladejo, J.; Shi, K.; Luo, X.; Yang, G.; Wu, T. A Review of Sludge-to-Energy Recovery Methods. *Energies* **2018**, *12*, 60. [[CrossRef](#)]
6. Cao, Y.; Pawłowski, A. Sewage sludge-to-energy approaches based on anaerobic digestion and pyrolysis: Brief overview and energy efficiency assessment. *Renew. Sustain. Energy Rev.* **2012**, *16*, 1657–1665. [[CrossRef](#)]
7. Tyagi, V.K.; Lo, S.-L. Sludge: A waste or renewable source for energy and resources recovery? *Renew. Sustain. Energy Rev.* **2013**, *25*, 708–728. [[CrossRef](#)]
8. Brethauer, S.; Studer, M.H. Biochemical Conversion Processes of Lignocellulosic Biomass to Fuels and Chemicals—A Review. *Chimia* **2015**, *69*, 572. [[CrossRef](#)]
9. Elorf, A.; Sarh, B.; Tabet, F.; Bostyn, S.; Asbik, M.; Bonnamy, S.; Chaoufi, J.; Boushaki, T.; Gillon, P. Effect of Swirl Strength on the Flow and Combustion Characteristics of Pulverized Biomass Flames. *Combust. Sci. Technol.* **2019**, *191*, 629–644. [[CrossRef](#)]

10. Gao, N.; Kamran, K.; Quan, C.; Williams, P.T. Thermochemical conversion of sewage sludge: A critical review. *Prog. Energy Combust. Sci.* **2020**, *79*, 100843. [CrossRef]
11. Bennini, M.; Koukouch, A.; Bakhattar, I.; Asbik, M.; Boushaki, T.; Sarh, B.; Elorf, A.; Cagnon, B.; Bonnamy, S. Characterization and Combustion of Olive Pomace in a Fixed Bed Boiler: Effects of Particle Sizes. *Int. J. Heat Technol.* **2019**, *37*, 229–238. [CrossRef]
12. Hu, X.; Gholizadeh, M. Biomass pyrolysis: A review of the process development and challenges from initial researches up to the commercialisation stage. *J. Energy Chem.* **2019**, *39*, 109–143. [CrossRef]
13. Shahbeig, H.; Nosrati, M. Pyrolysis of municipal sewage sludge for bioenergy production: Thermo-kinetic studies, evolved gas analysis, and techno-socio-economic assessment. *Renew. Sustain. Energy Rev.* **2020**, *119*, 109567. [CrossRef]
14. Mphahlele, K.; Matjie, R.H.; Osifo, P.O. Thermodynamics, kinetics and thermal decomposition characteristics of sewage sludge during slow pyrolysis. *J. Environ. Manag.* **2021**, *284*, 112006. [CrossRef] [PubMed]
15. Criado, J.M. Kinetic analysis of DTG data from master curves. *Thermochim. Acta* **1978**, *24*, 186–189. [CrossRef]
16. Fonts, I.; Azuara, M.; Gea, G.; Murillo, M.B. Study of the pyrolysis liquids obtained from different sewage sludge. *J. Anal. Appl. Pyrolysis* **2009**, *85*, 184–191. [CrossRef]
17. Naqvi, S.R.; Tariq, R.; Hameed, Z.; Ali, I.; Taqvi, S.A.; Naqvi, M.; Niazi, M.B.K.; Noor, T.; Farooq, W. Pyrolysis of high-ash sewage sludge: Thermo-kinetic study using TGA and artificial neural networks. *Fuel* **2018**, *233*, 529–538. [CrossRef]
18. Zhai, Y.; Peng, W.; Zeng, G.; Fu, Z.; Lan, Y.; Chen, H.; Wang, C.; Fan, X. Pyrolysis characteristics and kinetics of sewage sludge for different sizes and heating rates. *J. Therm. Anal. Calorim.* **2012**, *107*, 1015–1022. [CrossRef]
19. Shao, J.; Yan, R.; Chen, H.; Wang, B.; Lee, D.H.; Liang, D.T. Pyrolysis Characteristics and Kinetics of Sewage Sludge by Thermogravimetry Fourier Transform Infrared Analysis. *Energy Fuels* **2008**, *22*, 38–45. [CrossRef]
20. Park, E.-S.; Kang, B.-S.; Kim, J.-S. Recovery of Oils With High Caloric Value and Low Contaminant Content By Pyrolysis of Digested and Dried Sewage Sludge Containing Polymer Flocculants. *Energy Fuels* **2008**, *22*, 1335–1340. [CrossRef]
21. Chanaka Udayanga, W.D.; Veksha, A.; Giannis, A.; Lisak, G.; Lim, T.-T. Effects of sewage sludge organic and inorganic constituents on the properties of pyrolysis products. *Energy Convers. Manag.* **2019**, *196*, 1410–1419. [CrossRef]
22. *ASTM D5142-90*; Standard Test Methods for Proximate Analysis of the Analysis Sample of Coal and Coke by Instrumental Procedures. ASTM International: West Conshohocken, PA, USA, 1998.
23. *ASTM D2015-19*; Standard Test Method for Gross Calorific Value of Coal and Coke by the Adiabatic Bomb Calorimeter. ASTM International: West Conshohocken, PA, USA, 2019.
24. Dhyani, V.; Bhaskar, T. Kinetic Analysis of Biomass Pyrolysis. In *Waste Biorefinery*; Elsevier: Amsterdam, The Netherlands, 2018; pp. 39–83. Available online: <https://linkinghub.elsevier.com/retrieve/pii/B9780444639929000021> (accessed on 24 November 2022).
25. Yao, Z.; Yu, S.; Su, W.; Wu, W.; Tang, J.; Qi, W. Kinetic studies on the pyrolysis of plastic waste using a combination of model-fitting and model-free methods. *Waste Manag. Res.* **2020**, *38* (Suppl. S1), 77–85. [CrossRef]
26. Yao, Z.; Reinmüller, M.; Ortuño, N.; Zhou, H.; Jin, M.; Liu, J.; Luque, R. Thermochemical conversion of waste printed circuit boards: Thermal behavior, reaction kinetics, pollutant evolution and corresponding controlling strategies. *Prog. Energy Combust. Sci.* **2023**, *97*, 101086. [CrossRef]
27. Boundzanga, H.M.; Cagnon, B.; Roulet, M.; De Persis, S.; Vautrin-UI, C.; Bonnamy, S. Contributions of hemicellulose, cellulose, and lignin to the mass and the porous characteristics of activated carbons produced from biomass residues by phosphoric acid activation. *Biomass Conv. Bioref.* **2022**, *12*, 3081–3096. [CrossRef]
28. Magdziarz, A.; Wilk, M.; Gajek, M.; Nowak-Woźny, D.; Kopia, A.; Kalembe-Rec, I.; Koziński, J.A. Properties of ash generated during sewage sludge combustion: A multifaceted analysis. *Energy* **2016**, *113*, 85–94. [CrossRef]
29. Folgueras, M.B.; Alonso, M.; Díaz, R.M. Influence of sewage sludge treatment on pyrolysis and combustion of dry sludge. *Energy* **2013**, *55*, 426–435. [CrossRef]
30. Jenkins, B.M.; Baxter, L.L.; Miles, T.R., Jr.; Miles, T.R. Combustion properties of Biomass. *Fuel Process. Technol.* **1998**, *54*, 17–46. [CrossRef]
31. Channiwala, S.A.; Parikh, P.P. A unified correlation for estimating HHV of solid, liquid and gaseous fuels. *Fuel* **2002**, *81*, 1051–1063. [CrossRef]
32. Putun, A. Rice straw as a bio-oil source via pyrolysis and steam pyrolysis. *Energy* **2004**, *29*, 2171–2180. [CrossRef]
33. Bakhattar, I.; Asbik, M.; Chater, H.; El Alami, K.; Aadnan, I.; Zegaoui, O.; Mouaky, A.; Koukouch, A.; Benzaouak, A. Physico-chemical and Thermal Characterization of Olive Pomace (Biomass). In Proceedings of the 2021 9th International Renewable and Sustainable Energy Conference (IRSEC), virtual event, 23–27 November 2021; pp. 1–6.
34. Arauzo, P.J.; Atienza-Martínez, M.; Ábrego, J.; Olszewski, M.P.; Cao, Z.; Kruse, A. Combustion Characteristics of Hydrochar and Pyrochar Derived from Digested Sewage Sludge. *Energies* **2020**, *13*, 4164. [CrossRef]
35. Wang, Y.; Jia, L.; Guo, J.; Wang, B.; Zhang, L.; Xiang, J.; Jin, Y. Thermogravimetric analysis of co-combustion between municipal sewage sludge and coal slime: Combustion characteristics, interaction and kinetics. *Thermochim. Acta* **2021**, *706*, 179056. [CrossRef]
36. Bakhattar, I.; Asbik, M.; Koukouch, A.; Aadnan, I.; Zegaoui, O.; Blandria, V.; Bonnamy, S.; Sarh, B. Physicochemical characterization, thermal analysis and pyrolysis kinetics of lignocellulosic biomasses. *Biofuels* **2023**, *14*, 1–12. [CrossRef]
37. Böke, H.; Akkurt, S.; Özdemir, S.; Göktürk, E.H.; Caner Saltik, E.N. Quantification of CaCO_3 - $\text{CaSO}_3 \cdot 0.5\text{H}_2\text{O}$ - $\text{CaSO}_4 \cdot 2\text{H}_2\text{O}$ mixtures by FTIR analysis and its ANN model. *Mater. Lett.* **2004**, *58*, 723–726. [CrossRef]
38. Al-Hosney, H.A.; Grassian, V.H. Water, sulfur dioxide and nitric acid adsorption on calcium carbonate: A transmission and ATR-FTIR study. *Phys. Chem. Chem. Phys.* **2005**, *7*, 1266. [CrossRef] [PubMed]

39. Vali, N.; Åmand, L.-E.; Combres, A.; Richards, T.; Pettersson, A. Pyrolysis of Municipal Sewage Sludge to Investigate Char and Phosphorous Yield together with Heavy-Metal Removal—Experimental and by Thermodynamic Calculations. *Energies* **2021**, *14*, 1477. [[CrossRef](#)]
40. Lin, Y.; Liao, Y.; Yu, Z.; Fang, S.; Lin, Y.; Fan, Y.; Peng, X.; Ma, X. Co-pyrolysis kinetics of sewage sludge and oil shale thermal decomposition using TGA–FTIR analysis. *Energy Convers. Manag.* **2016**, *118*, 345–352. [[CrossRef](#)]
41. Barneto, A.G.; Carmona, J.A.; Alfonso, J.E.M.; Blanco, J.D. Kinetic models based in biomass components for the combustion and pyrolysis of sewage sludge and its compost. *J. Anal. Appl. Pyrolysis* **2009**, *86*, 108–114. [[CrossRef](#)]
42. Zhang, H.-Y.; Krafft, T.; Gao, D.; Zheng, G.-D.; Cai, L. Lignocellulose biodegradation in the biodrying process of sewage sludge and sawdust. *Dry. Technol.* **2018**, *36*, 316–324. [[CrossRef](#)]
43. Chen, Y.; Yang, H.; Zhao, Z.; Zou, H.; Zhu, R.; Jiang, Q.; Sun, T.; Li, M.; Li, L.; Shi, D.; et al. Comprehensively evaluating the digestive performance of sludge with different lignocellulosic components in mesophilic anaerobic digester. *Bioresour. Technol.* **2019**, *293*, 122042. [[CrossRef](#)]
44. Li, B.; Wei, W. Effect of lignin on the co-pyrolysis of sludge and cellulose. *Energy Sources Part A Recovery Util. Environ. Eff.* **2016**, *38*, 1825–1831. [[CrossRef](#)]
45. Miskolczi, N.; Tomasek, S. Investigation of Pyrolysis Behavior of Sewage Sludge by Thermogravimetric Analysis Coupled with Fourier Transform Infrared Spectrometry Using Different Heating Rates. *Energies* **2022**, *15*, 5116. [[CrossRef](#)]
46. Bonnamy, S. Carbonization of various precursors. Effect of heating rate Part II: Transmission electron microscopy and physico-chemical studies. *Carbon* **1999**, *37*, 1707–1724. [[CrossRef](#)]
47. Gabbott, P. (Ed.) *Principles and Applications of Thermal Analysis*; Blackwell Pub: Oxford, IA, USA, 2008; ISBN 978-1-4051-3171-1.
48. Magdziarz, A.; Werle, S. Analysis of the combustion and pyrolysis of dried sewage sludge by TGA and MS. *Waste Manag.* **2014**, *34*, 174–179. [[CrossRef](#)]
49. Thrower, P.A.; Radovic, L.R. *Chemistry & Physics of Carbon*; CRC Press: Boca Raton, FL, USA, 1999; ISBN 978-0-8247-1953-1.
50. Colpani, D.; Santos, V.O.; Araujo, R.O.; Lima, V.M.R.; Tenório, J.A.S.; Coleti, J.; Chaar, J.S.; de Souza, L.K.C. Bioenergy potential analysis of Brazil nut biomass residues through pyrolysis: Gas emission, kinetics, and thermodynamic parameters. *Clean. Chem. Eng.* **2022**, *1*, 100002. [[CrossRef](#)]
51. Koga, N.; Vyazovkin, S.; Burnham, A.K.; Favregeon, L.; Muravyev, N.V.; Perez-Maqueda, L.A.; Saggese, C.; Sánchez-Jiménez, P.E. ICTAC Kinetics Committee recommendations for analysis of thermal decomposition kinetics. *Thermochim. Acta* **2022**, *719*, 179384. [[CrossRef](#)]
52. Zong, P.; Jiang, Y.; Tian, Y.; Li, J.; Yuan, M.; Ji, Y.; Chen, M.; Li, D.; Qiao, Y. Pyrolysis behavior and product distributions of biomass six group components: Starch, cellulose, hemicellulose, lignin, protein and oil. *Energy Convers. Manag.* **2020**, *216*, 112777. [[CrossRef](#)]
53. Cai, J.; He, Y.; Yu, X.; Banks, S.W.; Yang, Y.; Zhang, X.; Yu, Y.; Liu, R.; Bridgwater, A.V. Review of physicochemical properties and analytical characterization of lignocellulosic biomass. *Renew. Sustain. Energy Rev.* **2017**, *76*, 309–322. [[CrossRef](#)]
54. Halikia, I.; Zoumpoulakis, L.; Christodoulou, E.; Prattis, D. Kinetic study of the thermal decomposition of calcium carbonate by isothermal methods of analysis. *Eur. J. Miner. Process. Environ. Prot.* **2001**, *1*, 89–102.
55. Ninan, K.N.; Krishnan, K.; Krishnamurthy, V.N. Kinetics and mechanism of thermal decomposition of insitu generated calcium carbonate. *J. Therm. Anal.* **1991**, *37*, 1533–1543. [[CrossRef](#)]
56. Rasool, T.; Srivastava, V.C.; Khan, M.N.S. Bioenergy Potential of *Salix alba* Assessed Through Kinetics and Thermodynamic Analyses. *Process Integr. Optim. Sustain.* **2018**, *2*, 259–268. [[CrossRef](#)]
57. Ahmad, M.S.; Mehmood, M.A.; Liu, C.-G.; Tawab, A.; Bai, F.-W.; Sakdaronnarong, C.; Xu, J.; Rahimuddin, S.A.; Gull, M. Bioenergy potential of *Wolffia arrhiza* appraised through pyrolysis, kinetics, thermodynamics parameters and TG-FTIR-MS study of the evolved gases. *Bioresour. Technol.* **2018**, *253*, 297–303. [[CrossRef](#)]

Disclaimer/Publisher’s Note: The statements, opinions and data contained in all publications are solely those of the individual author(s) and contributor(s) and not of MDPI and/or the editor(s). MDPI and/or the editor(s) disclaim responsibility for any injury to people or property resulting from any ideas, methods, instructions or products referred to in the content.